POLITECNICO DI TORINO
Repository ISTITUZIONALE

Easily sortable PHBH films functionalized via a magnetic Layer-by-Layer coating deposition

Original
Easily sortable PHBH films functionalized via a magnetic Layer-by-Layer coating deposition / Papatola, F., Damonte, G., Abba, L., Slimani, S., Carosio, F., Peddis, D., Monticelli, O., Pellis, A.. - In: REACTIVE & FUNCTIONAL POLYMERS. - ISSN 1381-5148. - 223:(2026). [10.1016/j.reactfunctpolym.2026.106711]

Availability:
This version is available at: 11583/3009108 since: 2026-03-24T11:02:18Z

Publisher:
Elsevier

Published
DOI:10.1016/j.reactfunctpolym.2026.106711

Terms of use:

This article is made available under terms and conditions as specified in the corresponding bibliographic description in the repository

Publisher copyright

(Article begins on next page)

02 November 2026

Reactive and Functional Polymers 223 (2026) 106711

Contents lists available at ScienceDirect

Reactive and Functional Polymers

journal homepage: www.elsevier.com/locate/react

Easily sortable PHBH films functionalized via a magnetic Layer-by-Layer coating deposition

Francesco Papatola [a], Giacomo Damonte [a], Lorenza Abbà [c], Sawssen Slimani [a,b], Federico Carosio [c], Davide Peddis [a,b], Orietta Monticelli [a,*], Alessandro Pellis [a,*]

[a] Università di Genova, Dipartimento di Chimica e Chimica Industriale, Via Dodecaneso 31, 16146 Genova, Italy
[b] CNR, Istituto di Struttura della Materia, nM^2-Lab, Monterotondo Scalo, Roma 00015, Italy
[c] Dipartimento di Scienza Applicata e Tecnologia, Politecnico di Torino-sede di Alessandria, viale Teresa Michel, 5, Alessandria 15121, Italy

ARTICLE INFO

Keywords:
Poly(3-hydroxybutyrate-*co*-3-hydroxyhexanoate) (PHBH)
Magnetic nanoparticles
Layer-by-Layer deposition
DNA
Chitosan
Enzymatic depolymerization

ABSTRACT

This work presents an eco-friendly and easily scalable process to modify the surface of poly(3-hydroxybutyrate-*co*-3-hydroxyhexanoate) (PHBH) films, a bioplastic of relevant application interest, making them magnetically active while preserving the intrinsic properties of the polymer. To achieve this, ~10 nm spinel iron oxide magnetic nanoparticles (MNPs), synthesized via coprecipitation method, were assembled using Layer-by-Layer (LbL) deposition with two bio-sourced polyelectrolytes: DNA (polyanion) and chitosan (polycation). An aminolysis reaction was employed to strengthen the interactions between the polymer substrate and the first coating layer. Additionally, the optimal reaction time was determined to maximize surface amine functionalization while minimizing film degradation. The effectiveness of the deposition was demonstrated by both the linear growth of the LbL assembly on a model silicon substrate using FT-IR measurements and by studying the morphology of the coated PHBH films through FE-SEM. These latter measurements showed the formation of a uniform coating after the deposition of 10 bilayers (BL). The 10 BL coated films demonstrated efficient magnetic separation from a mixed polymer waste scraps under a static applied magnetic field. Moreover, these materials undergo enzymatic degradation, with the MNPs that could be easily recovered from the enzymatic solution via magnetic separation, enabling their potential reuse. The proposed approach offers an alternative strategy aimed at tackling the issue of plastic contamination and material sorting during recycling.

1. Introduction

The exploitation of biodegradable polymers from renewable sources requires increasing efforts to modify their properties and thus expand their areas of application. Novel strategies that might enable the easy separation of these bio-based materials from other plastics (mostly fossil-based) during recycling are of fundamental importance to ensure an effective recycling of the polymeric materials. Another aspect that must be considered when developing bioplastics-based systems is the need to preserve their unique environmentally positive features such as their biodegradability. This work addresses all the above-mentioned aspects by focusing on a potentially large-scale applicable biopolymer, namely poly(3-hydroxybutyrate-*co*-3-hydroxyhexanoate) (PHBH). However, as for many bioplastics, the efficient separation and recovery of PHBH within conventional recycling streams remains a significant challenge. To address this limitation, the present work proposes a magnetically responsive approach for recycling applications by harnessing the potential of nanostructured magnetic materials into the end-of-life management of bioplastics, in line with previously proposed magnetic sorting strategies for plastics recovery [1,2]. The proposed strategy is not intended to replace existing waste management or recycling practices, but rather to complement them by enabling magnetic-based recovery. In this context, surface functionalization via Layer-by-Layer (LbL) assembly is explored as a versatile method to impart magnetic responsiveness while preserving the intrinsic biodegradability of the polymer. The possibility of magnetic field-based sorting could enhance the efficiency and purity of recycling streams, particularly in mixed or contaminated plastic waste scenarios.

The PHBH is a copolymer belonging to the polyhydroxyalkanoates (PHAs) family, consisting of two monomeric units: 3HB (3-hydroxybutyrate, short-chain unit) and 3HH (3-hydroxyhexanoate, medium-chain unit). When copolymerized, these monomers impart distinct

* Corresponding authors.
E-mail addresses: orietta.monticelli@unige.it (O. Monticelli), alessandro.pellis@unige.it (A. Pellis).

https://doi.org/10.1016/j.reactfunctpolym.2026.106711
Received 4 November 2025; Received in revised form 18 February 2026; Accepted 26 February 2026
Available online 27 February 2026
1381-5148/© 2026 The Authors. Published by Elsevier B.V. This is an open access article under the CC BY license (http://creativecommons.org/licenses/by/4.0/).

thermal and mechanical properties to the resulting polymer, improving the overall material performance when compared to other biopolymers. For example, the polyhydroxybutyrate that is obtained from the homopolymerization of 3-hydroxybutyrate units is biodegradable and has similar properties to polypropylene (PP) and low-density polyethylene (LDPE) [3], but suffers from processability constraints due to its high melting temperature and relatively low degradation temperature. On the other hand, 3HH, derived from 3-hydroxyhexanoic acid, displays a longer side chain than 3HB. This enhances the flexibility and toughness of PHBH by reducing crystallinity and lowering the melting point. Such features allow for a wider processing window with improved thermal stability [4]. In addition, by tailoring the composition of both highly crystalline (3HB) and elastomeric (3HH) units, PHBH copolymers can display tunable mechanical properties [5]. Therefore, thanks to its versatility, PHBH might find be employed in manufacturing processes such as: injection molding [6], extrusion [6,7], thermoforming [8,9], foaming [10], non-woven fabrics and fibers manufacturing [11,12], 3D printing [13], paper and fertilizer coating [14]. Besides the processing features, it is also important to consider some peculiar aspects related to the synthesis/availability of PHBH that make it an extremely promising biopolymer.

Indeed, PHBH is synthesized within various microorganisms, depending on factors like microorganism type, environmental conditions, and carbon sources such as amino acids, sugars, and fatty acids. Recently, advances in synthetic biology have led to the development of genetically engineered microorganisms, such as *Escherichia coli*, which can produce PHBH directly from glucose [15] or lauric acid [16], offering faster growth rates and easier purification compared to wild-type microorganisms [17]. Several companies, such as Kaneka Corporation in Japan, which is currently producing commercial PHBH grades, have demonstrated that large scale production and broad market introduction are possible [3]. It is therefore clear that further improvements in the functional properties of PHBH could expand its use as long as its specific characteristics are not altered, as previously underlined.

A possible strategy implies the use of a surface modification approach such as the Layer-by-Layer (LbL) technique, which is the method used in this work. The LbL assembly allows for the fabrication of multilayered coatings from the alternate adsorption from the liquid phase of two or more compounds characterized by a specific interaction. The electrostatic attraction occurring between polycations and polyanions in aqueous solutions is the most employed interaction. The simpler LbL assembly alternates two compounds in positively and negatively charged layers depositing, at each cycle, a bilayer (BL). The number of deposition cycles, and therefore BL, defines the thickness of the deposited coating [18]. The LbL assembly has gained considerable interest due to its versatility in coating design and its sustainable features [19], which rely on the use of water as a solvent and mild deposition conditions. In addition, by fine-tuning the deposition parameters, a plethora of components can be assembled to address a wide range of properties e.g. water repellency [20], controlled drug release [21,22], oxygen barrier [23], sensing [24], antimicrobial [25], and flame retardancy [26].

Beside polyelectrolytes, nanoparticles (NPs) can be easily implemented in a LbL assembly to improve the mechanical [27], thermal [28], and barrier properties [29] of the substrate. In recent years, the LbL approach has been widely applied to biopolymers such as polycaprolactone (PCL) [30,31] and polylactic acid (PLA) [32,33]. For the latter, the method was used to improve performance in areas such as drug delivery and food packaging. In particular, considering the use of nanoparticles, Li et al. combined graphite oxide nanoplatelets (GO) with chitosan or branched poly(ethylene imine) (BPEI) in order to improve hydrophilicity, reduce oxygen permeability, and provide antistatic properties [34]. Similarly, Carosio et al. improved the oxygen and water vapor barrier properties of PLA films incorporating a hydrophobic fluorinated polymer (Nafion) in a BPEI/NP assembly [35]. Although the above works demonstrate the feasibility of the LbL method to improve the properties of biopolymers, to the best of our knowledge to date, there is no evidence for the application of the LbL approach as a surface nanostructuring tool to further improve the performance and/or the properties of PHBH. Therefore, the novelty of this work is not uniquely related to the polymer matrix used, but also to the peculiar nature of the LbL assembly employed. The objective of the paper is to functionalize PHBH films to improve recycling by enabling magnetic field sorting procedures. To this end, a novel LbL assembly encompassing single-domain magnetic nanoparticles (MNPs) having a high saturation magnetization (Ms) was deposited on the surface of PHBH films using DNA and chitosan solutions as constituent polyelectrolytes and MNPs dispersing agents. The choice of DNA and chitosan as bio-sourced building blocks for the multilayer assembly by LbL was determined by their well-known self-assembly potential as well as by the possibility to target a sustainable coating composition. Therefore, in the proposed approach, the opposite charges of DNA (polyanion) and chitosan (polycation) are exploited to promote a LbL assembly by ionic interactions, while magnetic nanoparticles are *co*-dispersed in both solutions to ensure magnetic functionality without interfering with the electrostatic assembly process of polyelectrolytes [36,37]. The MNPs exhibit superparamagnetic behavior (i.e., characterized by zero remanent magnetization and coercivity) at room temperature and are biocompatible and environmentally safe [38]. The main advantage of this behavior is the absence of residual magnetism once the external magnetic field is removed. This prevents aggregation among the MNPs and avoids unintended magnetic attraction between film fragments and ferrous alloy components after the sorting procedure. In addition, unlike other LbL assembly strategies reported in the literature [39,40], where MNPs were used as one of the two charged compounds constituting the bilayer, this study presents a LbL strategy that ensures the homogeneous integration of the MNPs therefore maximizing the magnetic functionality within the coating without compromising its LbL electrostatic assembly. The procedure adopted to modify the PHBH-based films consists of a preliminary surface activation of the polymer through a simple and mild aminolysis reaction, which can generate amino groups that can interact with the first DNA layer. Chitosan- and DNA-containing magnetic nanoparticles (DNA_MNPs/CH_MNPs system) were then alternately deposited with intermediate washing steps (Fig. 1). The produced systems were characterized in detail in terms of their morphological, thermal, and magnetic properties as well as their enzymatic hydrolysis.

2. Experimental

2.1. Materials and methods

The chemicals $FeCl_2{\cdot}4H_2O$ (98%), $FeCl_3{\cdot}6H_2O$ (97%), HCl (37%), ammonium hydroxide (30%) for MNPs synthesis, chitosan (CH, $M_w \sim$ 190.000–310.000 g/mol, deacetylation degree ≥75%, viscosity 200–800 cps for c = 1% in 1% acetic acid), deoxyribonucleic acid (DNA, from herring sperm, crude oligonucleotides, < 50 base pairs, water ≤10%), acetic acid (glacial, ≥99%), ethylenediamine (ED, ≥99%), isopropanol (≥99.8%), dichloromethane (≥99.9%, 50–150 ppm amylene as stabilizer), and ninhydrin (ACS reagent grade) were purchased from Sigma-Aldrich and used as received. Poly(3-hydroxybutyrate-*co*-3-hydroxyhexanoate) (PHBH) IamNature B6 A15 C (melt mass flow rate (MFR) at 165 °C, 5 kg load = 6 g/10 min) was purchased by Gruppo MAIP (Italy). *Humicola insolens* Cutinase (HiC) (Novozym 51032, product code: 06-3135) was purchased from STREM Chemicals and used as received.

2.1.1. Preparation of PHBH films

PHBH thin films were prepared by casting 10 mL of a polymer solution in dichloromethane (PHBH concentration: 20 mg/mL) into a Petri dish (internal diameter: 54 mm). The dishes were left in the oven overnight at 30 °C to allow solvent evaporation. The resulting films were subsequently detached and vacuum-dried at 10 mbar and room

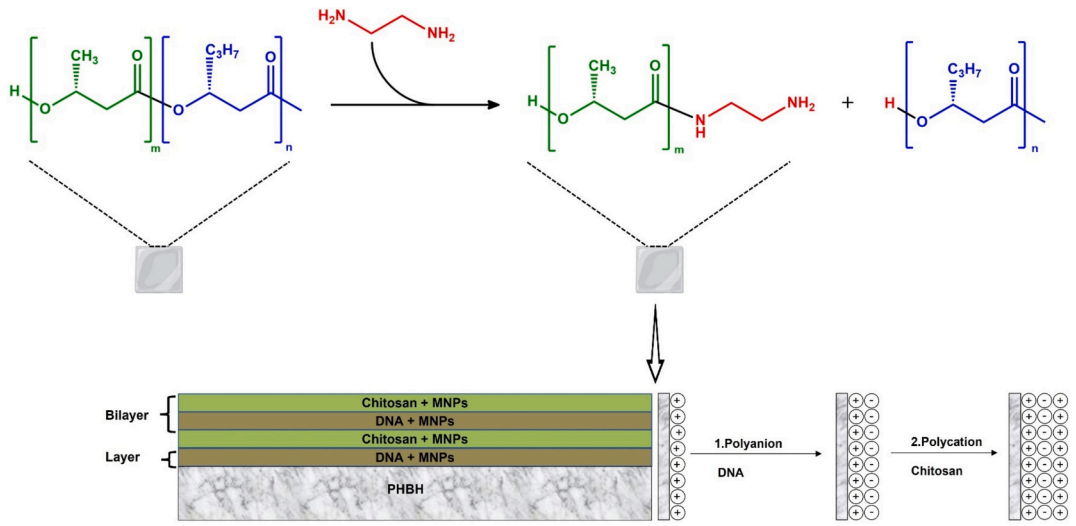


Fig. 1. Schematic overview of the LBL deposition process on PHBH based film.

temperature until constant weight was reached (6 days). After drying, the films (mean thickness = 40 ± 4 μm) were stored at room temperature in a desiccator over activated 4 Å molecular sieves.

2.1.2. Aminolysis of PHBH films

To provide the surface of the PHBH films with amino functional groups, 25 × 25 mm^2 samples were individually immersed in 25 mL of a 5% ED solution in isopropanol at 30 °C for 2 h in a 50-mL Falcon™ tube, using an orbital shaker at 200 rpm. After this treatment, the film samples were removed and washed with 25 mL Milli-Q/isopropanol solution (1:1 *v*/v) for 5 min, changing the liquid after each period for 1 h. The aminolyzed film samples (coded as PHBH_0) were then dried overnight at room temperature and directly employed for the LbL deposition process.

2.1.3. Ninhydrin assay

The presence of amino groups on the PHBH film surface was investigated using ninhydrin assay following the method reported by García-García et al. [41] Specifically, ninhydrin binds to amino groups present on the films producing a purple pigment with a maximum absorption at a wavelength of 560 nm in the solvent mixture chloroform/isopropanol (1:1), which can be detected and quantified using UV–Visible spectrophotometry. For this test, 3 PHBH film disks (diameter = 16 mm) were immersed in 1 M ninhydrin solution, developed in an oven at 70 °C for 15 min, and dissolved in 1 mL of chloroform/isopropanol (1:1) mixture before analysis. The resulting solution was then ultracentrifuged at 14500 rpm for 10 min, and the clear supernatant analyzed by UV–Vis spectrophotometry.

2.1.4. Spinel iron oxide nanoparticles

Spinel iron oxide magnetic nanoparticles were synthesized using the co-precipitation method using an aqueous solution of Fe^{2+} and Fe^{3+} ions in a 1:2 stoichiometric ratio, followed by alkalinization with 30% ammonia solution [42]. The synthesis was carried out according to the following procedure: a mixture of $FeCl_3{\cdot}6H_2O$ (>99%) and $FeCl_2.4H_2O$ (>99%) was dissolved in 100 mL 0.01 M HCl solution (98%) at 60 °C. The solution was then alkalinized by adding a 30% ammonium hydroxide solution. After two hours of magnetic stirring, the resulting precipitate was collected by magnetic separation and washed three times with deionized water. The X-ray diffraction pattern (Fig. S1) shows reflections typical of the iron phase with spinel structure (JCPDS card No.75-449). Any extra phase has been detected, and the average crystallite size of 9.0 (1) nm was estimated by the Scherrer equation [43].The obtained black powder was dried overnight in an oven at 60 °C prior to its use in the LbL deposition process.

2.1.5. LBL deposition

Bilayers (BL) were deposited by successive dipping of aminolyzed PHBH films (PHBH_0) in aqueous DNA and chitosan (CH) solution, both prepared at a concentration of 0.5% (*w*/w). DNA solutions exhibited a pH of approximately 2.6, while chitosan was dissolved by the addition of 0.25% (*v*/v) acetic acid, resulting in a mildly acidic environment (pH ~ 4.4) and ensuring protonation of its amino groups. An amount of 1% (*w*/*v*) magnetic nanoparticles was added to the DNA and chitosan solutions. Before the LbL deposition, the DNA_MNPs and CH_MNPs solutions were sonicated (5 min; RT; 40 kHz) to promote MNPs dispersion and mixing with the medium. Moreover, the PHBH films were alternately dipped in the DNA (polyanion) and CH (polycation) solutions while being continuously agitated in an orbital shaker (from VWR, KS 3000 I control model). The first DNA layer was achieved by dipping the film in the DNA solution (5 min) and then rinsing with Milli-Q water (1 min) to remove the excess solution. The CH layer was applied using the same procedure to create a BL. The procedure was repeated until the desired number of BL was reached (5, 10, 15, and 20). The samples were coded according to the number of deposited BL (e.g., PHBH_10 indicates 10 BL of DNA and CH deposited onto an aminolyzed PHBH_0 film). Dynamic light scattering (DLS) was employed to measure the zeta potential (ζ) and hydrodynamic size (d_H) of MNPs dispersed in Milli-Q water (pH = 7.4 ± 0.4), as well as DNA and CH solutions, and the corresponding DNA_MNPs and CH_MNPs mixtures. These measurements allow to investigate the interfacial properties and interaction dynamics between the individual components.

2.1.6. Enzymatic hydrolysis

Enzymatic hydrolysis of films was performed by placing single film specimens (PHBH_10, 5 × 8 mm^2, mean weight 9.0 mg, $n = 5$) in a 1.5 mL Eppendorf tube, followed by 1 mL HiC solution (5 μM, in Potassium Phosphate buffer, KPO, 0.1 M at pH = 8.0). The film samples were then incubated at 50 °C in an oven. At the specified time, the film residues were removed manually, washed three times by immersion in 1 mL ultrapure water each time, and vacuum-dried at room temperature for three days until constant weight was reached. The weight loss of specimens was determined gravimetrically on an analytical scale (accuracy: ±0.0001 g).

2.2. Characterization techniques

2.2.1. FT-IR analysis

The growth of the LbL assembly up to 10 BL was monitored on a model silicon wafer substrate [(100), single side polished] using a Fourier transform infrared (FT-IR) spectrophotometer (16 scans and 4 cm^{-1} resolution, Frontier, Perkin Elmer) in transmission mode. After each deposition step, the Si wafer was dried, and IR spectra of the deposited layers were collected. Attenuated total reflectance (ATR) FT-IR spectroscopy spectra for the neat, aminolyzed, and coated PHBH films were collected at room temperature in the 4000–400 cm^{-1} (16 scans and 4 cm^{-1} resolution) range using an FT-IR spectrophotometer (Frontier, Perkin Elmer, Italy) equipped with Germanium crystal.

2.2.2. DSC measurements

Differential Scanning Calorimeter (DSC) thermograms for the neat, aminolyzed, and coated PHBH-based films (approx. 5.0 ± 1.0 mg) were measured using a Mettler Toledo "DSC1 STAR^e System®" in the temperature range from −100 to 150 °C, with heating and cooling performed at a rate of 10 °C/min under a nitrogen flow of 20 mL/min.

2.2.3. TGA analysis

To investigate the effect of the number of bilayers on the thermal stability of the resulting films, all the samples up to 20 BL were analyzed by thermogravimetric analysis (TGA) using a Mettler Toledo "TGA/DSC1 STAR^e System®" micro and ultra-micro balances with sub-microgram resolution over the whole measurement range. Each sample (approx. 8.0 ± 1.0 mg), placed into alumina pans, was measured under an 80 mL/min nitrogen flow and heated from 30 to 800 °C at a heating rate of 10 °C/min.

2.2.4. FE-SEM analysis

SEM analysis of the sample morphology (surface and cross-section) was performed using a Zeiss Supra 40 VP field emission scanning electron microscope (FE-SEM) equipped with a backscattered electron detector. Before analysis, the films were sputter-coated with carbon using a Polaron E5100 sputter coater.

2.2.5. WCA analysis

Water contact angle (WCA) measurements were performed using an Attension® Theta tensiometer using ultrapure distilled water at 22 °C. To determine the contact angle value (θ), film specimens were stuck to microscopy glass slides using bi-adhesive tape, and static contact angles were determined by analyzing a minimum of six drops (volume = 3 μL) for each film sample.

2.2.6. XRD analysis

The crystalline structure of MNPs was characterized by X-ray diffraction (XRD) measurements, using a TT 3003 diffractometer equipped with a secondary graphite monochromator and CuKα radiation (λ = 1.5418 Å). The data were recorded in the 10° − 90° 2θ range with a step size of 0.04° and a counting time of 4 s per step.

2.2.7. Magnetic measurements

The field dependence of magnetization was investigated, using a vibrating sample magnetometer (VSM Model 10–Microsense) equipped with an electromagnet generating a magnetic field in the range of ∓2 T. All the magnetic measurements were normalized by the mass of the magnetic phase, and the saturation magnetization value was determined using the approach to saturation law (LAS) [44] at high fields.

2.2.8. ^1H NMR analysis

^1H NMR analysis of the starting PHBH was performed on PHBH solution ($CDCl_3$, 30 mg/mL 25 °C) using a Bruker Avance 500 MHz spectrometer (Bruker, Karlsruhe, Germany). The mean numerical molecular weight and the comonomer composition of PHBH were determined using the equations reported elsewhere [45].

2.2.9. Magnetic separation

A neodymium-iron-boron (NdFeB) commercial magnet with a defined magnetic strength (max.operation temperature = 60 °C; Flux inside the magnet = 1.4299 Tesla; Length = 50 mm; Width = 30 mm; Height = 20 mm; Holding force on iron = 81.72 Newton) was used to evaluate the magnetic responsiveness of the magnetic films. A separation test was performed by mixing pieces (approximately 1 × 1 cm^2) of the magnetically functionalized PHBH film (aminolyzed and coated with 20 bilayers) with untreated commercial plastic pieces (including polylactic acid, PLA; polyethylene terephthalate (PET) and polypropylene (PP)).

3. Results and discussions

The present work focused on the surface modification of films based on poly(3-hydroxybutyrate-*co*-3-hydroxyhexanoate) (PHBH), which consists of 89% 3-oxobutyric units and 11% 3-oxohexanoic units (Fig. S2), as determined by ^1H NMR [45], using the LbL method for the first time on this type of polymer. The dense PHBH films were prepared by solvent casting and functionalized by an aminolysis reaction to obtain the proper surface functional groups, namely ionizable amino groups that are positively charged at acidic or neutral pH. These groups were used to ionically interact with the components of the DNA solution (DNA_MNPs), owing to their opposite negative charges, leading to the deposition of a first negatively charged DNA/MNPs surface layer. This initial layer served as a primer for the LbL growth. The subsequent immersion in a CH-based solution containing MNPs (CH_MNPs), with both CH and MNPs having a positive charge, resulted in the deposition of a second, positively charged CH/MNPs layer to form the first BL. The successive alternate deposition of multiple DNA- and CH-based layers led to their LbL assembly (DNA_MNPs/CH_MNPs systems) eventually producing LbL functionalized PHBH-based films. The combination of magnetic nanoparticles with both DNA and CH was selected to ensure their incorporation into both types of layers, allowing for a more homogeneous distribution throughout the multilayer structure. With this approach, the polyelectrolytes not only drive the electrostatic LbL growth, but also act as efficient carriers of the MNPs, enabling their stable integration and uniform distribution within the coating while imparting magnetic functionality to the resulting film.

3.1. Study of the surface functionalization of PHBH-based films

The work was preliminary focused on the surface functionalization of PHBH films carried out by aminolysis using a 5% (*v*/v) solution of ED in isopropanol, a reaction generally applied for the functionalization of polyesters with diamines and involving a nucleophilic attack of the ED amino groups on the PHBH ester bonds, leading to the formation of free amino and hydroxyl groups on the film surface [41,46]. It is worth underlining that this reaction, which has been widely used for the modification of polyesters such as PLA and PCL [47,48], has only been described in very few works performed on PHBH [41,49]. Since aminolysis leads to a progressive decrease in the molecular weight of the surface polymer chains, resulting in material erosion over time [41], the first step was to determine the optimal reaction conditions to achieve adequate surface functionalization without causing significant deterioration of the film. Therefore, the manipulability of the materials was evaluated after different contact times with ED solution (1, 2, 3, and 4 h) by manually bending the films with tweezers (Fig. S3). After 4 h of aminolysis, a partial embrittlement of the materials was observed, which precluded further use. Due to this phenomenon, which can be attributed to polymer degradation triggered by aminolysis [48], it was decided to focus the study on the film functionalized by adopting a reaction time of 2 h (coded as PHBH_0), to limit embrittlement while ensuring the surface functionalization. The validation of the surface functionalization of

the films treated with ED for 2 h was investigated using different techniques such as FT-IR, WCA, and ninhydrin assay. No difference was observed when comparing the FT-IR spectra of the neat film with the aminolyzed one, probably due to a low presence of amine and amide groups on the surface of the films, which may be below the instrumental detection limit and cannot be revealed with this technique (Fig. S4). Nevertheless, WCA measurements of the films before and after the aminolysis treatment (Fig. 2a and b respectively) revealed a strong decrease in the contact angle value (θ) from about 100° for the pristine material to 65° for PHBH_0, which is consistent with the findings reported by other authors for similar systems [50]. This reduction, indicating an increase in the surface hydrophilicity of the material, indirectly points to the presence of hydrophilic functional groups on the film surface. To confirm the presence and quantify the number of amino functionalities formed on the film surface, the neat system and the ED-treated system were exposed to a ninhydrin solution to develop specific staining, which was subsequently quantified by spectrophotometric analysis. While the neat PHBH film was characterized by negligible content of amino groups, which was below the instrumental detection limit, the analysis of PHBH_0 revealed an -NH_2 concentration of 6.9 ± 0.3 10^{-2} μmol/cm^2. This clear difference in the amino group content of the two investigated systems (Fig. 2a and b) supports the effectiveness of the aminolysis reaction. Moreover, it was found that this value corresponds to what is reported in the literature for other PHBH films functionalized by aminolysis reaction with a dendrimeric poly(amidoamine) (PAMAM) [49].

To evaluate the influence of the aminolysis reaction on film morphology and thermal properties, SEM, DSC, and TGA measurements were performed. Regarding the latter analysis, TGA and DTG (Fig. 2e and f) revealed a slightly different thermal stability of the investigated samples. The onset decomposition temperature (T_{onset}) and the temperature of the maximum decomposition rate (T_{max}) were reduced by 10 °C for the film subjected to the ED treatment. These results can be attributed to the reduction in the molecular weight of the surface polymer chains. Nevertheless, it can be assumed that such slight decrease in thermal stability does not affect the subsequent deposition process as well as the material application [51]. These results were strongly supported by the DSC analyses (Fig. S5 and Table S1), which showed an increase in both the melting enthalpy (ΔH_m) and degree of crystallinity (χ_c) of the films during the first heating run, rising from 50 Jg^{-1} and 34% for PHBH to 61 Jg^{-1} and 42% for PHBH_0. This difference was also observed during the second heating phase of the film as a decrease in the cold crystallization enthalpy (ΔH_{cc}) and an increase in ΔH_m values. This variation can be ascribed to the presence of low-molecular-weight chains on the film surface formed during the aminolysis step, which have greater mobility than the pristine high-molecular-weight chains and are therefore characterized by a higher tendency to structure [52].

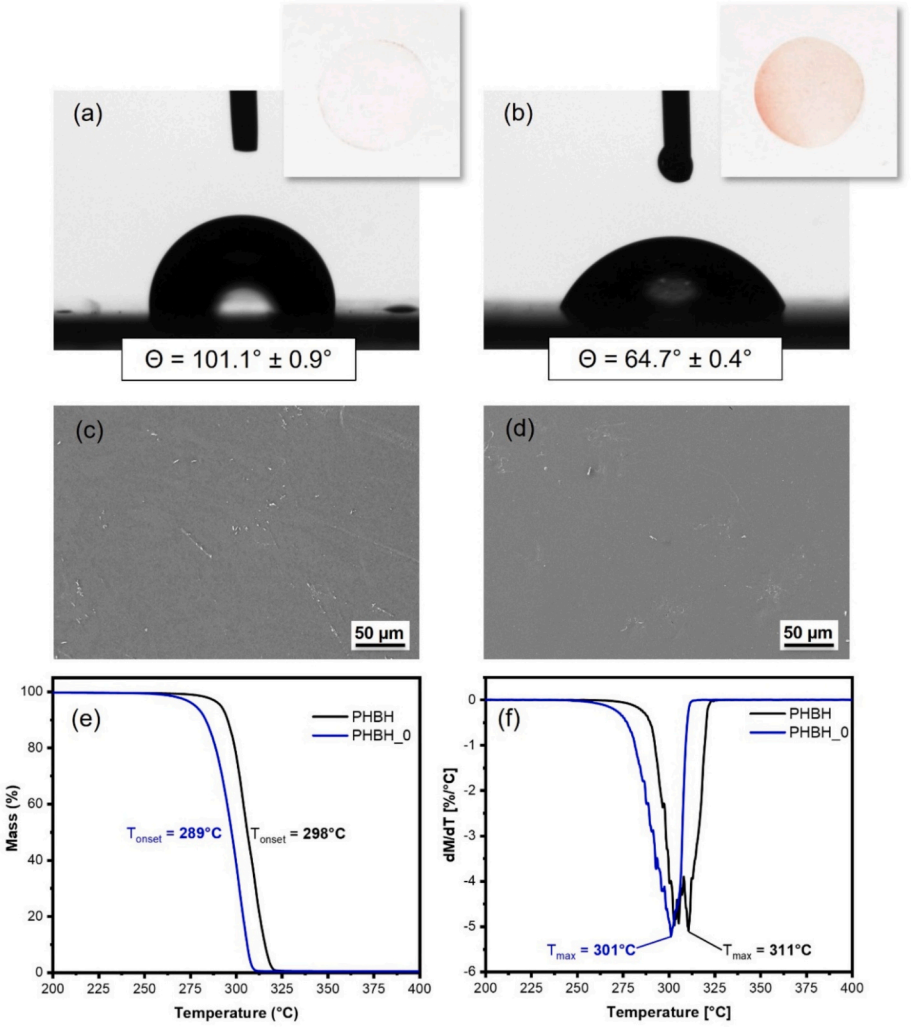


Fig. 2. Characterization of PHBH-based films surface functionalization: WCA measurements of PHBH films before (a) and after aminolysis (b) with the corresponding photographs of PHBH films after treatment with ninhydrin solution and development at 70 °C before (left) and after (right) 2 h of aminolysis; SEM micrographs of PHBH (c) and PHBH_0 (d); TGA (e) and DTG (f) analysis of PHBH and PHBH_0.

Despite the slight modification in the thermal properties of the aminolyzed film, SEM analysis showed no significant changes in its surface morphology compared to the starting sample (Fig. 2c and d). This result, which differs from that of some other treated films based on PHBH and other polyesters that showed significant surface erosion as a result of the aminolysis reaction [41], can be attributed to various aspects related to both the aminolysis conditions (time, temperature, reagent concentration) and the characteristics of the treated materials (molecular weight, crystallinity, film thickness, etc.). Therefore, while a direct comparison with the results reported in the literature is difficult, SEM results highlight that the film functionalization, confirmed by other techniques, affects only a limited thickness of the system surface.

3.2. Investigation of MNPs-containing dispersions

Uncoated Iron oxide nanoparticles were selected because of their natural ability to reversibly change their surface charge depending on the pH of the medium and counter-ions [53], making them ideal building blocks for electrostatically driven LbL assemblies. Specifically, the colloidal stability of MNPs in aqueous media is primarily influenced by pH-dependent surface charge, driven by the protonation and deprotonation of surface hydroxyl groups [54]. At low pH, the surface is dominated by positively charged Fe-OH_2^+ groups, which gradually transform into neutral (Fe-OH) and into negatively charged (Fe—O^-) forms in neutral and basic conditions, respectively. As confirmed by DLS measurements (Fig. 3a), the point of zero charge (PZC) for the system under investigation was identified at pH ~ 7.5, in agreement with previous studies [55], and associated with a clear tendency for nanoparticles' agglomeration. When MNPs are introduced into the DNA solution (pH ~ 2.6), the phosphate backbone retained its negative charge due to the low pK_a values of phosphate groups (< 2) [56], resulting in a strong electrostatic attraction between the negatively charged DNA and the positively charged MNPs (Fe-OH_2^+) under acidic conditions. This interaction was confirmed by zeta potential measurements: the DNA_MNPs complex exhibited a less negative value ($\zeta = -24.5$ mV $\pm \sigma = 5.5$ mV) than DNA alone ($\zeta = -35.3$ mV $\pm \sigma = 4.1$ mV), indicating a partial charge neutralization upon attraction (Fig. 3b). Conversely, when MNPs were dispersed into CH solution (pH ~ 4.4), both components carried positive surface charges (Fe-OH_2^+ and NH_3^+, respectively), which would normally lead to electrostatic repulsion.

However, chitosan is known to coordinate metal oxide surfaces via its unprotonated amine and hydroxyl functionalities, enabling complex formation even under repulsive electrostatic conditions [57]. Indeed, some works support the formation of such complexes over a wide pH range where chitosan amines are only partially protonated, particularly between pH 4 and 6 [57]. This coordination-driven interaction led to a further increase in surface charge, with the CH_MNPs complex showing a ζ value of +78.2 mV ± σ = 5.8 mV, compared to +67.3 mV ± σ = 4.3 mV for CH alone (Fig. 3b). The pronounced charge difference between DNA ($\zeta \sim -35$) and CH ($\zeta \sim +67$ mV) supports the feasibility of a LbL approach. This promotes efficient polyelectrolyte adsorption during the alternate deposition cycles, enhancing the coating assembly. Meanwhile, both the polyanionic and polycationic components contribute to successful incorporation of MNPs into the multilayered structure on PHBH films, which occurs through a combination of electrostatic and coordination interaction under carefully controlled pH conditions.

3.3. Study of neat and LbL modified PHBH-based films

To clearly demonstrate the chemical change in the PHBH-based films after the LbL deposition, the IR spectrum of the aminolyzed film (PHBH_0) was compared with those of CH, DNA and a coated film treated with the highest BL number, namely 20 (PHBH_20) (Fig. S6).

In the spectrum of PHBH_0, a strong, sharp, and steep band was observed at 1719 cm^{-1} corresponding to the C═O stretching vibration [58]. Other characteristic signals for PHBH were also visible approximately at 1274, 1180, and 1054 cm^{-1}, ascribed to ester groups in the polymer structure. Furthermore, PHBH exhibited peaks at 978, 1227, and 1262 cm^{-1}, associated with the crystalline phase of the film, while bands at 2871, 2931, and 2977 cm^{-1} were attributed to CH stretching, asymmetric stretching of CH_2, and C-CH_3, respectively [59]. As far as the PHBH_20 is concerned, the above characteristic peaks disappeared and the signals ascribed to both DNA and CH (Fig. S7a and b respectively) were distinguished with some wavenumber and intensity variations due to their LbL assembly, as well as the characteristic band at 535 cm^{-1} corresponding to the Fe—O vibrations of MNPs is noticeable. In detail, the signal attributed to the C═O vibration of DNA nucleotide bases (1682 cm^{-1}) was broadened and shifted to a lower wavenumber (1635 cm^{-1}) due to the overlapping with the chitosan asymmetric and symmetric stretching vibrations of protonated amine groups (1640 and 1565 cm^{-1}, respectively). Moreover, PO^{2-} stretching vibrations (1210 cm^{-1}) were shifted towards lower wavenumbers (1200 cm^{-1}) due to the electrostatic interaction with NH_3^+ counterions attributed to chitosan (1150 cm^{-1}) in the LbL assembly, while the peak at 1057 cm^{-1} was attributed to the sum of the C-O-C stretching signals of both chitosan and DNA. These results point out the successful LbL assembly of the two biocomponents and MNPs on the surface of the PHBH-based film.

The growth of DNA_MNPs/CH_MNPs assembly was monitored as a function of BL deposited on PHBH by recording the IR-ATR spectra of the films coated with 5, 10, 15, and 20 BL (PHBH_5, PHBH_10, PHBH_15, and PHBH_20, respectively) (Figs. S8a and S9).

The evolution of the two more intense peaks at 1564 cm^{-1} and 955

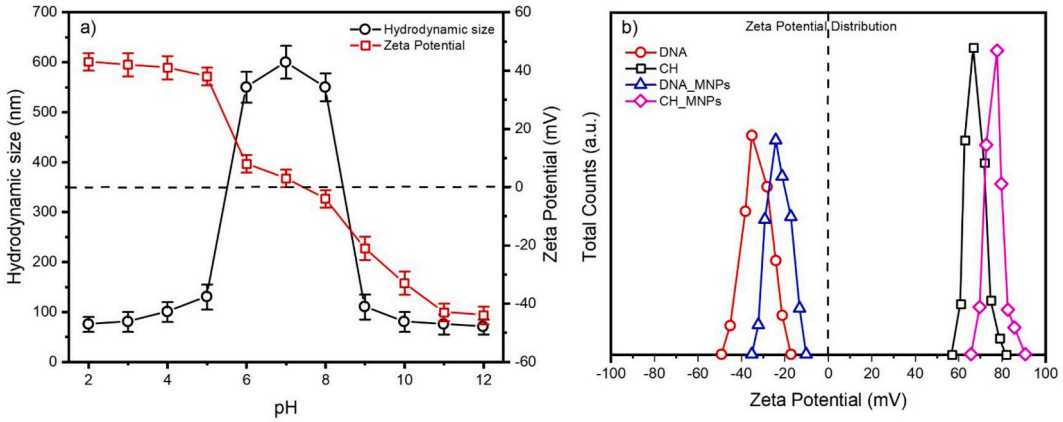


Fig. 3. DLS measurements: a) Zeta potential and Hydrodynamic size of magnetite (MNPs) to assess the PZC. Each condition was measured in triplicate, and the error bars represented the standard deviations; b) Zeta potential distribution of DNA (red circles), CH (black square), DNA_MNS (blue triangles) and CH (magenta rhombus). (For interpretation of the references to colour in this figure legend, the reader is referred to the web version of this article.)

cm^{-1} as a function of the deposited BL was also followed, demonstrating that the coating growth reached a plateau above 10 BL, as the intensity of the two peaks showed no significant changes in the samples with 10,15 and 20 BL (Fig. S8b). Moreover, Fig. S10 provides additional evidence for the beneficial role of aminolysis in improving the electrostatic affinity between the substrate surface and the initially deposited DNA layer, as the film without any functionalization reaction displayed no evidence of MNPs deposition after a LbL treatment with 10 BL.

The thermal stability of the aminolyzed PHBH film and the LbL-treated films was evaluated by thermogravimetric analysis (TGA) in inert atmosphere, comparing the thermograms with those of the neat biocomponents and the MNPs (Fig. S11). As well documented in the literature [60], the decomposition of CH occurred in a single, well-defined step between 250 and 400 °C, releasing H_2O, NH_3, CO, CO_2, and CH_3COOH, producing a carbonaceous residue that is subsequently slowly and continuously converted into polyaromatic structures (final residual mass ~ 10%). Furthermore, according to reports on DNA [61], an abrupt mass drop was observed near 220 °C, due to the chemical decomposition of phosphate groups and the release of phosphoric acid (final residual mass ~ 40%). As observed in the thermogram of MNPs, magnetite is stable over the entire temperature range, as expected for Fe_3O_4 nanoparticles [62]. In the TGA thermograms (Fig. 4), T_{max} showed no significant differences between PHBH_0 and LBL-treated systems with 5, 10, 15 and 20 BL, T_{max} being ~284 °C for PHBH_0 and ~286 °C for all coated films.

When the DNA_MNPs/CH_MNPs system was assembled, the resulting films still exhibited a single-step thermal decomposition, which was slightly anticipated with respect to aminolyzed PHBH film, as shown by the T_{onset} (~272 °C and 276 °C for PHBH_0 and PHBH_5, respectively, vs ~ 268 °C for all the other LBL assemblies). The final residual mass for PHBH_0 was 0%, while for PHBH_5, PHBH_10, PHBH_15, and PHBH_20 was 19, 41, 47, and 48%, respectively, pointing out an increased amount of CH- and DNA-containing magnetic nanoparticles successfully deposited on the surface of the PHBH films. However, it should be noted that these residual masses also reflect different weight losses associated with the contribution of physically adsorbed water on aminolyzed film which was released at low temperatures. To better emphasize the contribution of the deposited multilayers on dry-ash-free basis, the residual mass was recalculated by normalizing the weight at 100 °C to 100%. Under these conditions, the final residual mass for PHBH_5, PHBH_10, PHBH_15, and PHBH_20 was 18, 39, 44, and 45%. Interestingly, the residual mass increase shows diminishing returns above 10 BL thus pointing out a somewhat plateau in the deposition process.

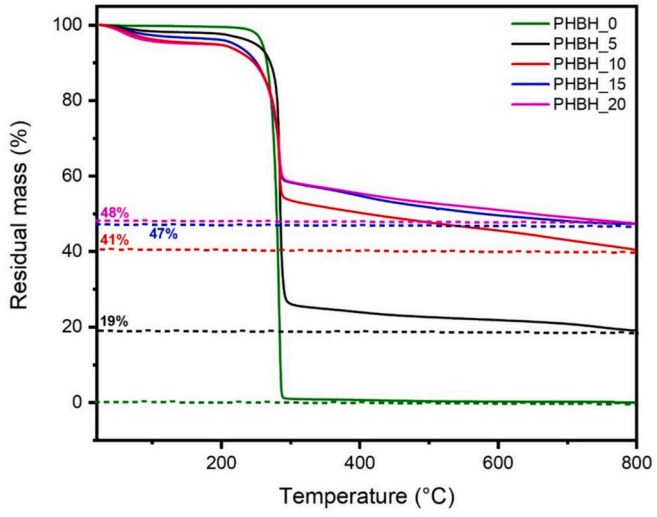


Fig. 4. TGA curve of PHBH_0 and LBL assemblies with 5, 10, 15, and 20 BL (PHBH_5, PHBH_10, PHBH_15, and PHBH_20, respectively).

The effect of the number of deposited layers on the magnetic properties was investigated by comparing the magnetic behavior of bare MNPs, the aminolyzed PHBH film, and LbL modified films containing up to 20 DNA_MNPs/CH_MNPs-based BL. The field dependence of magnetization at 300 K (Fig. 5a) revealed a superparamagnetic behavior (i.e., coercive field, H_c, and remanent magnetization, M_r, equal to 0), consistent with previously reported results on spinel iron oxide nanoparticles with similar particle size (10 nm) [63,64], while the aminolyzed PHBH substrate displayed a diamagnetic response (Fig. S12).

The M_s was found to increase progressively with the number of layers, indicating a corresponding increase in the amount of MNPs deposited onto the PHBH surface as the coating thickness increased. Notably, as illustrated in the inset of Fig. 5a, the Ms. value of the PHBH_20 film (55 ± 3 Am^2/kg) was nearly identical to that of the bare MNPs (58 ± 2 Am^2/kg) within experimental error. This suggests that additional depositions beyond 20 layers would result in minimal enhancement of magnetization. These findings demonstrate that the developed LbL assembly technique effectively imparts magnetic responsiveness to the PHBH films through the surface deposition of DNA_MNPs/CH_MNPs multilayers. The resulting M_s values are sufficiently high to allow efficient separation of the films from non-magnetic polymer materials under an applied static magnetic field, as shown in the supporting video (Video S1a and S1b). Upon approaching the magnet, the attraction and selective separation of the magnetically treated films from the other plastic materials were qualitatively observed, demonstrating the feasibility of magnetic field assisted separation. This capability offers promising potential to improve the efficiency and purity of plastic recycling processes by addressing major challenges such as contamination and the separation of mixed plastic waste (Fig. 5b and c).

Based on the above results, it can be concluded that both TGA and VSM analysis confirmed a limited LbL growth above 10 BL, as shown in Fig. 6. Therefore, limited differences were observed in the final residual mass and M_s values of PHBH films coated with 10, 15, and 20 BL of DNA_MNPs/CH_MNPs system (PHBH_10, PHBH_15, and PHBH_20, respectively) (Table S2). Contrary to what has been reported in the literature for DNA/CH LbL systems [37], where the coating growth displayed a two regimes of linear growth after 10 BL, the presence of MNPs in the present assembly lead to a plateau condition with limit in the growth profile of the coating. This can be ascribed to the formation, during the deposition of 15 and 20 BL, of a highly swollen assembly that limits the coating growth by weaking interactions among the deposited layers that can be either partially or totally removed upon washing.

FE-SEM analysis was performed on films coated by 5 and 10 BL (referred to as PHBH_5 and PHBH_10) (Fig. 7). In PHBH_5, areas of exposed substrate alternate with zones where the deposition of the DNA_MNPs/CH_MNPs assembly is clearly visible. In contrast, PHBH_10 exhibited a continuous coating over the entire film surface, with no uncoated regions, suggesting that the deposition of 10 BL was sufficient to achieve complete and homogeneous substrate coverage. Moreover, the cross-section analysis of the samples shown in Fig. 7c and d confirmed that the thickness and homogeneity of the deposited DNA_MNPs/CH_MNPs assembly increased with the number of BL, which was consistent with the IR-ATR measurements reported in the previous section (Fig. S8). Analysis of the SEM micrographs also showed that the deposited coating adhered well to the PHBH substrate (Fig. S13), a phenomenon indicative of the good electrostatic interactions between the positively charged amino groups on the film surface and the negatively charged DNA-based solution constituting the first deposited layer.

3.4. Study of LbL growth on model silicon substrate

To better investigate the assembly of the DNA_MNPs/CH_MNPs system, the growth of the coating was monitored on a model silicon substrate using FT-IR spectroscopy. The deposition up to 10 BL was investigated, as this is the limit found for the PHBH-based films.

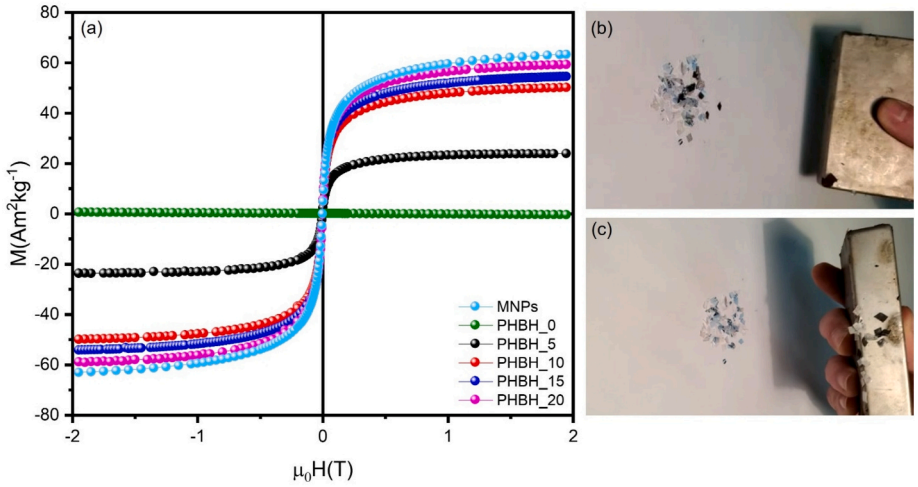


Fig. 5. (a) Field dependence of magnetization recorded at 300 K for bare MNPs, aminolysis-treated PHBH film before (PHBH_0) and after 5,10, 15, and 20 depositions of DNA_MNPs/CH_MNPs system (PHBH_5, PHBH_10, PHBH_15, and PHBH_20, respectively); sequential images, extracted from supporting information (Video S1a), showing magnetic separation tests of PHBH_20 from a heterogeneous plastics group before (b) and after (c) the application of the magnetic device.

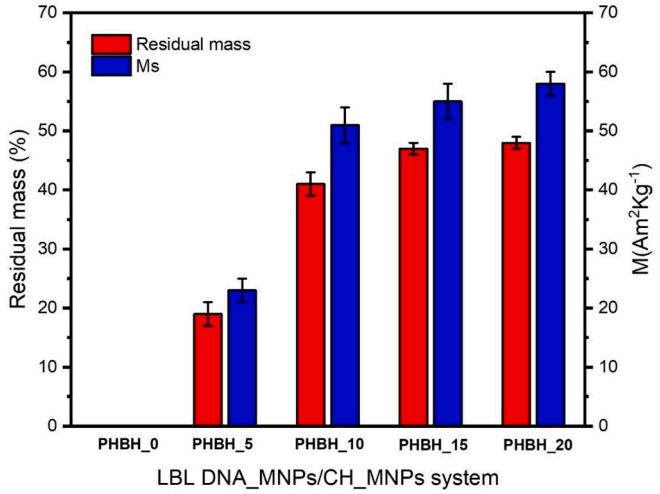


Fig. 6. Progression of final residual mass and M_s values of PHBH films after 10,15, and 20 BL (PHBH_10, PHBH_15, and PHBH_20, respectively).

The LbL growth was graphically represented by a 3D graph (Fig. 8), showing the IR spectra as a function of the BL numbers. Additionally, a magnification of the IR from 1800 to 900 cm^{-1} is given in Fig. 8b, allowing for a clearer view of this specific region where the main peaks of the assembly can be easily observed. Indeed, the characteristic peaks ascribed to P═O, PO^{2-} and P-O-C groups of the phosphate deoxyribose backbone are visible at 1225 and 969 cm^{-1}, while signals due to C═C and C═N stretching modes (namely, at 1538, 1485, 1421, and 1374 cm^{-1}) confirmed the presence of pyrimidine and purine bases in the DNA_MNPs/CH_MNPs assembly [37]. In all the spectra, including the one collected at low BL, it was possible to observe that the broad peak around 3372 cm^{-1}, associated to the O—H stretching typical of both DNA and CH, overlapped with the stretching of.

amino groups (3550–3330 cm^{-1}) and the shoulder at 2959 cm^{-1} was assigned to C—H bond of CH [65]. The strong signal at 1696 cm^{-1} was attributed to the C═O vibration of guanine, cytosine, and thymine [37], while the peak at 1067 cm^{-1} was ascribed to the C-O-C stretching vibrations of both DNA backbone and of chitosan pyranose rings [34,66], as seen in Fig. S7c. The characteristic peak at 546 cm^{-1}, corresponding to the Fe—O vibrations of spinel iron oxide nanoparticles is also visible [67]. To investigate the trend of IR signal evolution as a function of deposited BL, the two more specific peaks at 1067 cm^{-1} and 1696 cm^{-1} were monitored. These specific peaks were found to increase linearly with the number of deposited BL (Fig. 8c), as previously demonstrated for DNA/CH-based systems [34,35]. Furthermore, comparing the spectra of DNA_MNPs/CH_MNPs assembly with those of the neat components, it was clear that the signals associated with DNA (i.e., 1696 and 1225 cm^{-1}) were more intense than the CH ones, indicating the formation of a DNA-rich coating (Fig. S14).

3.5. *Enzymatic hydrolysis of films*

To investigate the behavior of a system coated with the LbL method towards enzymatic hydrolysis, the weight of a film brought into contact with a solution of *Humicola insolens* cutinase (HiC), an enzyme that is highly active in the hydrolysis of many polyesters [68,69], and that has also demonstrated significant hydrolytic activity towards PHAs [45], was monitored over time. The enzymatic hydrolysis of the films coated with 10 BL (PHBH_10) was performed using a 5 μM HiC solution in KPO 0.1 M buffer (pH = 8.0) at 50 °C. This sample was selected because 10 BL ensure a homogeneous coating and approach a plateau in MNPs deposition.

As can be seen from the histogram in Fig. S15, the mass loss of the films increased dramatically after two days, from 9% to 77% after 24 and 48 h of immersion, which can be related to the complete detachment of the coating from the samples, as also evidenced in Fig. S16. This phenomenon can be explained by the different behavior towards enzymatic hydrolysis of the deposited layer and the polymer substrate, as already demonstrated in another work [36]. Interestingly, the detached material based on superparamagnetic MNPs can be easily separated using a neodymium magnet, avoiding additional time-consuming centrifugation and/or filtration steps (Fig. S17). After 40 days of immersion, the residual film mass loss reached 84%, confirming the intrinsic susceptibility of PHBH to HiC-mediated hydrolysis. Overall, these findings demonstrate that these materials can be selectively disassembled into their components, i.e., MNPs and PHBH, under mild conditions, enabling environmentally friendly and efficient recovery.

4. Conclusions

In this study, a Layer-by-Layer (LbL) approach was successfully used to modify poly(3-hydroxybutyrate-*co*-3-hydroxyhexanoate) (PHBH)-based films. The developed method consisted in the deposition of alternating layers of DNA and chitosan (CH) embedded with MNPs on

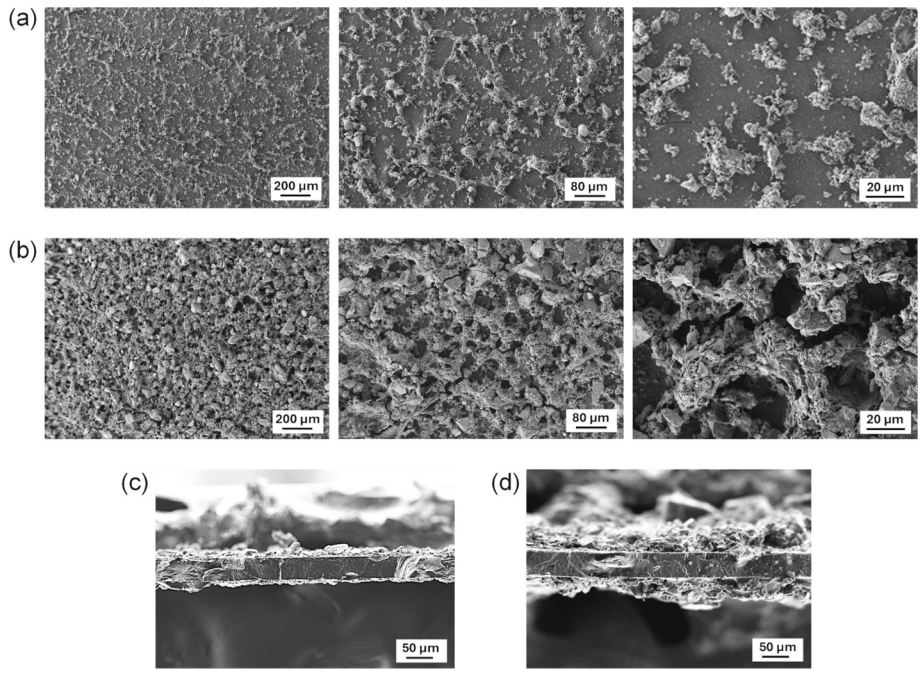


Fig. 7. SEM micrographs at different magnifications of PHBH_5 (a) and PHBH_10 (b) and their corresponding cross-sections (c and d).

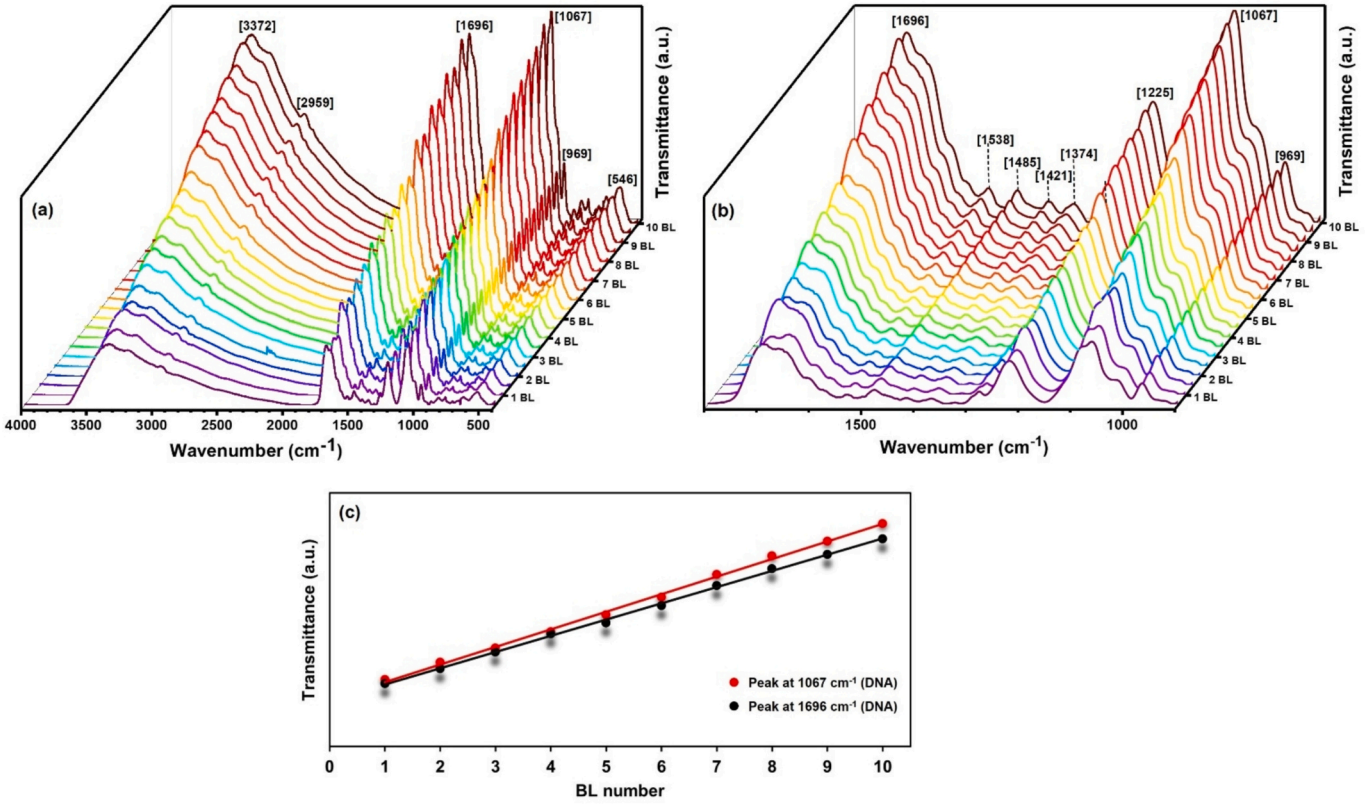


Fig. 8. (a) 3D IR spectrum growth on model silicon wafer substrate in the range of 4000–400 cm^{-1}; (b) Zoom in the range 1800–900 cm^{-1}; (c) Evolution of the signals at 1067 cm^{-1} as function of BL number.

the surface of the polymer films, activated by an aminolysis reaction, which enabled an efficient LbL assembly and produced an adherent multilayer coating. The characterization of the multilayer growth and morphology confirmed the progressive and uniform build-up of this DNA_MNPs/CH_MNPs assembly, with a linear growth up to 10 bilayers (BL) beyond which a plateau was observed, indicating a saturation in the deposition process. The deposition of 10 bilayers (BL) effectively conferred magnetic properties to PHBH films, enabling efficient separation from other polymer materials and addressing the persistent challenge of contamination and material sorting. Moreover, the coating

was found to be removable upon exposure to an enzymatic solution, allowing for the biodegradation of the film and the recovery—and potential reuse—of the magnetic nanoparticles (MNPs) via a static magnetic field. Scaling up of the proposed system would primarily require magnetic devices of appropriate dimensions to handle higher material throughput. However, industrial implementation would require a careful techno-economic evaluation. Future upscaling efforts should include a cost-effectiveness as well as a life-cycle assessment (LCA) to evaluate the environmental impact of the large-scale process.

Supplementary data to this article can be found online at https://doi.org/10.1016/j.reactfunctpolym.2026.106711.

CRediT authorship contribution statement

Francesco Papatola: Writing – review & editing, Writing – original draft, Methodology, Investigation, Formal analysis, Data curation, Conceptualization. **Giacomo Damonte:** Writing – review & editing, Visualization, Methodology, Investigation, Conceptualization. **Lorenza Abbà:** Writing – review & editing, Methodology, Investigation, Formal analysis. **Sawssen Slimani:** Writing – review & editing, Supervision, Investigation. **Federico Carosio:** Writing – review & editing, Visualization, Supervision, Data curation. **Davide Peddis:** Writing – review & editing, Validation, Supervision. **Orietta Monticelli:** Writing – review & editing, Writing – original draft, Validation, Supervision, Formal analysis, Conceptualization. **Alessandro Pellis:** Writing – review & editing, Visualization, Validation, Supervision, Resources, Project administration, Funding acquisition, Conceptualization.

Declaration of competing interest

The authors declare no competing financial interests.

Acknowledgements

Funded by the European Union (ERC, CIRCULARIZE, 101114664). Views and opinions expressed are, however, those of the author(s) only and do not necessarily reflect those of the European Union or the European Research Council. Neither the European Union nor the granting authority can be held responsible for them.

Data availability statement

All data supporting the findings of this study are available within the article or its supplementary materials.

References

[1] G. Houzeaux, C. Samaniego, H. Calmet, R. Aubry, M. Vázquez, P. Rem, Simulation of magnetic fluid applied to plastic sorting, Open Waste Manag. J. 3 (2014) 127–138, https://doi.org/10.2174/1876400201003010127.
[2] Y. Ueda, F. Mishima, Y. Akiyama, S. Nishijima, Fundamental study of plastic separation utilizing magnetic force, IEEE Trans. Appl. Supercond. 24 (2014) 1–5, https://doi.org/10.1109/TASC.2013.2292306.
[3] K. Eraslan, C. Aversa, M. Nofar, M. Barletta, A. Gisario, R. Salehiyan, Y.A. Goksu, Poly(3-hydroxybutyrate-co-3-hydroxyhexanoate) (PHBH): synthesis, properties, and applications - a review, Eur. Polym. J. 167 (2022) 111044, https://doi.org/10.1016/j.eurpolymj.2022.111044.
[4] R. Turco, G. Santagata, I. Corrado, C. Pezzella, M. Di Serio, In vivo and post-synthesis strategies to enhance the properties of PHB-based materials: a review, Front. Bioeng. Biotechnol. 8 (2021) 619266, https://doi.org/10.3389/fbioe.2020.619266.
[5] C.Y. Loo, K. Sudesh, Polyhydroxyalkanoates: bio-based microbial plastics and their properties, Malays. Polym. J. 2 (2007) 31–57.
[6] D.Z. Bucci, L.B.B. Tavares, I. Sell, PHB packaging for the storage of food products, Polym. Test. 24 (2005) 564–571, https://doi.org/10.1016/j.polymertesting.2005.02.008.
[7] J.J. Fischer, Y. Aoyagi, M. Enoki, Y. Doi, T. Iwata, Mechanical properties and enzymatic degradation of poly ([R]-3-hydroxybutyrate-co-[R]-3-hydroxyhexanoate) uniaxially cold-drawn films, Polym. Degrad. Stab. 83 (2004) 453–460, https://doi.org/10.1016/j.polymdegradstab. 2003.08.006.
[8] E.L. Sánchez-Safont, A. Aldureid, J.M. Lagarón, L. Cabedo, J. Gámez-Pérez, Study of the compatibilization effect of different reactive agents in PHB/natural fiber-based composites, Polymers (Basel) 12 (2020) 1967, https://doi.org/10.3390/polym12091967.
[9] E.L. Sanchez-Safont, L. Cabedo, J. Gamez-Perez, Cellulose-reinforced biocomposites based on PHB and PHBV for food packaging applications, in: Sustain. Food Packag. Technol., 2021, pp. 225–261, https://doi.org/10.1002/9783527820078.ch8.
[10] N. Le Moigne, M. Sauceau, M. Benyakhlef, R. Jemai, J.-C. Bénézet, E. Rodier, J.-M. Lopez-Cuesta, J. Fages, Foaming of poly (3-hydroxybutyrate-co-3-hydroxyvalerate)/organo-clays nano-biocomposites by a continuous supercritical CO2 assisted extrusion process, Eur. Polym. J. 61 (2014) 157–171, https://doi.org/10.1016/j.eurpolymj.2014.10.008.
[11] M.-L. Cheng, P.-Y. Chen, C.-H. Lan, Y.-M. Sun, Structure, mechanical properties and degradation behaviors of the electrospun fibrous blends of PHBHHx/PDLLA, Polymer (Guildf) 52 (2011) 1391–1401, https://doi.org/10.1016/j.polymer.2011.01.039.
[12] T. Kabe, C. Hongo, T. Tanaka, T. Hikima, M. Takata, T. Iwata, High tensile strength fiber of poly [(R)-3-hydroxybutyrate-co-(R)-3-hydroxyhexanoate] processed by two-step drawing with intermediate annealing, J. Appl. Polym. Sci. 132 (2015), https://doi.org/10.1002/app.41258.
[13] C. Mota, S. Wang, D. Puppi, M. Gazzarri, C. Migone, F. Chiellini, G. Chen, E. Chiellini, Additive manufacturing of poly [(R)-3-hydroxybutyrate-co-(R)-3-hydroxyhexanoate] scaffolds for engineered bone development, J. Tissue Eng. Regen. Med. 11 (2017) 175–186, https://doi.org/10.1002/term.1897.
[14] S. Sängerlaub, M. Brüggemann, N. Rodler, V. Jost, K.D. Bauer, Extrusion coating of paper with poly(3-hydroxybutyrate-co-3-hydroxyvalerate) (PHBV)—packaging related functional properties, Coatings 9 (2019) 457, https://doi.org/10.3390/coatings9070457.
[15] Q. Wang, Y. Luan, X. Cheng, Q. Zhuang, Q. Qi, Engineering of Escherichia coli for the biosynthesis of poly (3-hydroxybutyrate-co-3-hydroxyhexanoate) from glucose, Appl. Microbiol. Biotechnol. 99 (2015) 2593–2602, https://doi.org/10.1007/s00253-015-6380-0.
[16] X. Lu, J. Zhang, Q. Wu, G.-Q. Chen, Enhanced production of poly(3-hydroxybutyrate-co-3-hydroxyhexanoate) via manipulating the fatty acid β-oxidation pathway in E. coli, FEMS Microbiol. Lett. 221 (2003) 97–101, https://doi.org/10.1016/S0378-1097(03)00173-3.
[17] S.Y. Lee, E. coli moves into the plastic age, Nat. Biotechnol. 15 (1997) 17–18, https://doi.org/10.1038/nbt0197-17b.
[18] G. Decher, Fuzzy nanoassemblies: toward layered polymeric multicomposites, Science (80-.) 277 (1997) 1232–1237, https://doi.org/10.1126/science.277.5330.1232.
[19] J.J. Richardson, J. Cui, M. Bjornmalm, J.A. Braunger, H. Ejima, F. Caruso, Innovation in layer-by-layer assembly, Chem. Rev. 116 (2016) 14828–14867, https://doi.org/10.1021/acs.chemrev.6b00627.
[20] J. Bravo, L. Zhai, Z. Wu, R.E. Cohen, M.F. Rubner, Transparent superhydrophobic films based on silica nanoparticles, Langmuir 23 (2007) 7293–7298, https://doi.org/10.1021/la070159q.
[21] P. Arnaldi, F. Carosio, D. Di Lisa, L. Muzzi, O. Monticelli, L. Pastorino, Assembly of chitosan-graphite oxide nanoplatelets core shell microparticles for advanced 3D scaffolds supporting neuronal networks growth, Colloids Surf. B Biointerfaces 196 (2020) 111295, https://doi.org/10.1016/j.colsurfb.2020.111295.
[22] X. Zhang, T. Liang, Q. Ma, Layer-by-Layer assembled nano-drug delivery systems for cancer treatment, Drug Deliv. 28 (2021) 655–669, https://doi.org/10.1080/10717544.2021.1905748.
[23] F. Li, P. Biagioni, M. Finazzi, S. Tavazzi, L. Piergiovanni, Tunable green oxygen barrier through layer-by-layer self-assembly of chitosan and cellulose nanocrystals, Carbohydr. Polym. 92 (2013) 2128–2134, https://doi.org/10.1016/j.carbpol.2012.11.091.
[24] Y. Ohno, K. Maehashi, K. Matsumoto, Label-free biosensors based on aptamer-modified graphene field-effect transistors, J. Am. Chem. Soc. 132 (2010) 18012–18013, https://doi.org/10.1021/ja108127r.
[25] S.T. Dubas, P. Kumlangdudsana, P. Potiyaraj, Layer-by-layer deposition of antimicrobial silver nanoparticles on textile fibers, Colloids Surf. A Physicochem. Eng. Asp. 289 (2006) 105–109, https://doi.org/10.1016/j.colsurfa.2006.04.012.
[26] X. Qiu, Z. Li, X. Li, Z. Zhang, Flame retardant coatings prepared using layer by layer assembly: a review, Chem. Eng. J. 334 (2018) 108–122, https://doi.org/10.1016/j.cej.2017.09.194.
[27] T.U. Patro, H.D. Wagner, Layer-by-layer assembled PVA/laponite multilayer free-standing films and theirmechanical and thermal properties, Nanotechnology 22 (2011) 455706, https://doi.org/10.1088/0957-4484/22/45/455706.
[28] M. Le Wu, Y. Chen, L. Zhang, H. Zhan, L. Qiang, J.N. Wang, High-performance carbon nanotube/polymer composite fiber from layer-by-layer deposition, ACS Appl. Mater. Interfaces 8 (2016) 8137–8144, https://doi.org/10.1021/acsami.6b01130.
[29] F. Ben Dhieb, E.J. Dil, S.H. Tabatabaei, F. Mighri, A. Ajji, Effect of nanoclay orientation on oxygen barrier properties of LbL nanocomposite coated films, RSC Adv. 9 (2019) 1632–1641, https://doi.org/10.1039/C8RA09522A.
[30] M. Labet, W. Thielemans, Synthesis of polycaprolactone: a review, Chem. Soc. Rev. 38 (2009) 3484–3504, https://doi.org/10.1039/B820162P.
[31] E. Malikmammadov, T.E. Tanir, A. Kiziltay, V. Hasirci, N. Hasirci, PCL and PCL-based materials in biomedical applications, J. Biomater. Sci. Polym. Ed. 29 (2018) 863–893, https://doi.org/10.1080/09205063.2017.1394711.
[32] L.-T. Lim, R. Auras, M. Rubino, Processing technologies for poly (lactic acid), Prog. Polym. Sci. 33 (2008) 820–852, https://doi.org/10.1016/j.progpolymsci.2008.05.004.
[33] V. Nagarajan, A.K. Mohanty, M. Misra, Perspective on polylactic acid (PLA) based sustainable materials for durable applications: focus on toughness and heat

resistance, ACS Sustain. Chem. Eng. 4 (2016) 2899–2916, https://doi.org/10.1021/acssuschemeng.6b00321.
[34] K. Li, A. Fina, D. Marrè, F. Carosio, O. Monticelli, Graphite oxide nanocoatings as a sustaibale route to extend the applicability of biopolymer-based film, Appl. Surf. Sci. 522 (2020) 146471, https://doi.org/10.1016/j.apsusc.2020.146471.
[35] F. Carosio, S. Colonna, A. Fina, G. Rydzek, J. Hemmerle, L. Jierry, P. Schaaf, F. Boulmedais, Efficient gas and water vapor barrier properties of thin poly (lactic acid) packaging films: functionalization with moisture resistant nafion and clay multilayers, Chem. Mater. 26 (2014) 5459–5466, https://doi.org/10.1021/cm501359e.
[36] L. Valle, L. Maddalena, G. Damonte, F. Carosio, A. Pellis, O. Monticelli, Biodegradable and gas barrier polylactic acid/star-shaped polycaprolactone blend films functionalized with a bio-sourced polyelectrolyte coating, Colloids Surf. B Biointerfaces 236 (2024) 113806, https://doi.org/10.1016/j.colsurfb.2024.113806.
[37] F. Carosio, A. Di Blasio, J. Alongi, G. Malucelli, Green DNA-based flame retardant coatings assembled through layer by layer, Polymer (Guildf.) 54 (2013) 5148–5153, https://doi.org/10.1016/j.polymer.2013.07.029.
[38] R.M. Cornell, U. Schwertmann, The Iron Oxides: Structure, Properties, Reactions, Occurrences and Uses, John Wiley & Sons, 2003, https://doi.org/10.1002/3527602097.
[39] M.A.G. Soler, L.G. Paterno, P.C. Morais, Layer-by-layer assembly of magnetic nanostructures, J. Nanofluids 1 (2012) 101–119, https://doi.org/10.1166/jon.2012.1015.
[40] I. Dincer, O. Tozkoparan, S.V. German, A.V. Markin, O. Yildirim, G.B. Khomutov, D.A. Gorin, S.B. Venig, Y. Elerman, Effect of the number of iron oxide nanoparticle layers on the magnetic properties of nanocomposite LbL assemblies, J. Magn. Magn. Mater. 324 (2012) 2958–2963, https://doi.org/10.1016/j.jmmm.2012.04.002.
[41] J.M. García-García, I. Quijada-Garrido, L. López, R. París, M.T. Núñez-López, E. De La Peña Zarzuelo, L. Garrido, The surface modification of poly(3-hydroxybutyrate-co-3-hydroxyhexanoate) copolymers to improve the attachment of urothelial cells, Mater. Sci. Eng. C 33 (2013) 362–369, https://doi.org/10.1016/j.msec.2012.08.052.
[42] S. Slimani, C. Meneghini, M. Abdolrahimi, A. Talone, J.P.M. Murillo, G. Barucca, N. Yaacoub, P. Imperatori, E. Illés, M. Smari, E. Dhahri, D. Peddis, Spinel iron oxide by the co-precipitation method: effect of the reaction atmosphere, Appl. Sci. 11 (2021), https://doi.org/10.3390/app11125433.
[43] M.E. Wieser, T.B. Coplen, Atomic weights of the elements 2009 (IUPAC technical report), Pure Appl. Chem. 83 (2010) 359–396, https://doi.org/10.1351/PAC-REP-10-09-14.
[44] A.H. Morrish, The Physical Principles of Magnetism, 2001, https://doi.org/10.1109/9780470546581.
[45] G. Damonte, M. Cozzani, M. Ozenda, C. Siracusa, M.J. Calandri, A. Pellis, G. M. Guebitz, O. Monticelli, Environmentally friendly upcycling of PHA-based copolymers, Int. J. Biol. Macromol. (2025) 145457, https://doi.org/10.1016/j.ijbiomac.2025.145457.
[46] O. Jeznach, D. Kołbuk, M. Marzec, A. Bernasik, P. Sajkiewicz, Aminolysis as a surface functionalization method of aliphatic polyester nonwovens: impact on material properties and biological response, RSC Adv. 12 (2022) 11303–11317, https://doi.org/10.1039/d2ra00542e.
[47] N. Rabiei, M.H. Kish, Aminolysis of polyesters for cracking and structure clarifying: a review, Polym. Adv. Technol. 33 (2022) 3903–3919, https://doi.org/10.1002/pat.5837.
[48] G. Damonte, R. Spotorno, D. Di Fonzo, O. Monticelli, Multifunctional porous films based on polylactic acid/polycaprolactone blend and graphite nanoplateles, ACS Appl. Polym. Mater. 4 (2022) 6521–6530, https://doi.org/10.1021/acsapm.2c00923.
[49] Q. Luo, F. Zou, D. Yang, Y. Huang, D. Xian, Y. Nie, Z. Zhang, Y. Zheng, Y. Liu, F. Zhou, P. Yang, Y. Jiang, X. Huang, X. Zou, The production and characterization of an aminolyzed polyhydroxyalkanoate membrane and its cytocompatibility with osteoblasts, Molecules 30 (2025) 950, https://doi.org/10.3390/molecules30040950.
[50] D. Garcia-Garcia, L. Quiles-Carrillo, R. Balart, S. Torres-Giner, M.P. Arrieta, Innovative solutions and challenges to increase the use of poly(3-hydroxybutyrate) in food packaging and disposables, Eur. Polym. J. 178 (2022) 111505, https://doi.org/10.1016/j.eurpolymj.2022.111505.
[51] G. Damonte, I. Zaborniak, M. Klamut, D. Di Lisa, L. Pastorino, K. Awsiuk, K. Wolski, P. Chmielarz, O. Monticelli, Development of functionalized poly(lactide) films with chitosan via SI-SARA ATRP as scaffolds for neuronal cell growth, Int. J. Biol. Macromol. 273 (2024) 132768, https://doi.org/10.1016/j.ijbiomac.2024.132768.
[52] O. Jeznach, D. Kolbuk, P. Sajkiewicz, Aminolysis of various aliphatic polyesters in a form of nanofibers and films, Polymers (Basel) 11 (2019) 1669, https://doi.org/10.3390/polym11101669.
[53] A. Talone, P. Maltoni, M. Casale, M. Abdolrahimi, S. Slimani, D. Colombara, L. Leoncino, P. Imperatori, S. Laureti, G. Varvaro, Novel formulation of ionic liquid-based ferrofluids: investigation of the magnetic properties, Langmuir 41 (2025) 11977–11986, https://doi.org/10.1021/acs.langmuir.5c00403.
[54] A.F.C. Campos, R. Aquino, F.A. Tourinho, F.L.O. Paula, J. Depeyrot, Influence of the spatial confinement at nanoscale on the structural surface charging in magnetic nanocolloids, Eur. Phys. J. E: Soft Matter Biol. Phys. 36 (2013) 42, https://doi.org/10.1140/epje/i2013-13042-y.
[55] M. Kosmulski, pH-dependent surface charging and points of zero charge. IV. Update and new approach, J. Colloid Interface Sci. 337 (2009) 439–448, https://doi.org/10.1016/j.jcis.2009.04.072.
[56] P. Thaplyal, P.C. Bevilacqua, Experimental approaches for measuring pKa's in RNA and DNA, in: Methods Enzymol., Elsevier, 2014, pp. 189–219, https://doi.org/10.1016/B978-0-12-801122-5.00009-X.
[57] R.B. Hernández, A.P. Franco, O.R. Yola, A. Lopez-Delgado, J. Felcman, M.A. L. Recio, A.L.R. Mercê, Coordination study of chitosan and Fe3+, J. Mol. Struct. 877 (2008) 89–99, https://doi.org/10.1016/j.molstruc.2007.07.024.
[58] Y. Zhou, Z. Huang, X. Diao, Y. Weng, Y.-Z. Wang, Characterization of the effect of REC on the compatibility of PHBH and PLA, Polym. Test. 42 (2015) 17–25, https://doi.org/10.1016/j.polymertesting.2014.12.014.
[59] R.A. Rebia, S. Rozet, Y. Tamada, T. Tanaka, Biodegradable PHBH/PVA blend nanofibers: fabrication, characterization, in vitro degradation, and in vitro biocompatibility, Polym. Degrad. Stab. 154 (2018) 124–136, https://doi.org/10.1016/j.polymdegradstab. 2018.05.018.
[60] I. Corazzari, R. Nisticò, F. Turci, M.G. Faga, F. Franzoso, S. Tabasso, G. Magnacca, Advanced physico-chemical characterization of chitosan by means of TGA coupled on-line with FTIR and GCMS: thermal degradation and water adsorption capacity, Polym. Degrad. Stab. 112 (2015) 1–9, https://doi.org/10.1016/j.polymdegradstab. 2014.12.006.
[61] J. Niziol, J. Fiedor, J. Pagacz, E. Hebda, M. Marzec, E. Gondek, I.V. Kityk, DNA-hexadecyltrimethyl ammonium chloride complex with enhanced thermostability as promising electronic and optoelectronic material, J. Mater. Sci. Mater. Electron. 28 (2017) 259–268, https://doi.org/10.1007/s10854-016-5519-9.
[62] E.T. Tenório-Neto, T. Jamshaid, M. Eissa, M.H. Kunita, N. Zine, G. Agusti, H. Fessi, A.E. El-Salhi, A. Elaissari, TGA and magnetization measurements for determination of composition and polymer conversion of magnetic hybrid particles, Polym. Adv. Technol. 26 (2015) 1199–1208, https://doi.org/10.1002/pat.3562.
[63] A.G. Roca, M.P. Morales, K. O'Grady, C.J. Serna, Structural and magnetic properties of uniform magnetite nanoparticles prepared by hightemperature decomposition of organic precursors, Nanotechnology 17 (2006) 2783, https://doi.org/10.1088/0957-4484/17/11/010.
[64] J.M.D. Coey, Magnetism and Magnetic Materials, Cambridge University Press, 2010.
[65] L. Abba, M. Marcioni, L. Maddalena, G. Sanchez-Olivares, F. Carosio, Fire safe and sustainable lightweight materials based on Layer-by-Layer coated keratin fibers from tannery wastes, J. Mater. Sci. Technol. 205 (2025) 150–158, https://doi.org/10.1016/j.jmst.2024.03.055ICAMS2024.
[66] G. Socrates, Infrared and Raman Characteristic Group Frequencies: Tables and Charts, John Wiley & Sons, 2004.
[67] W. Zhai, J. He, P. Han, M. Zeng, X. Gao, Q. He, Adsorption mechanism for tetracycline onto magnetic Fe3O4 nanoparticles: adsorption isotherm and dynamic behavior, location of adsorption sites and interaction bonds, Vacuum 195 (2022) 110634, https://doi.org/10.1016/j.vacuum.2021.110634.
[68] V. Ferrario, A. Pellis, M. Cespugli, G.M. Guebitz, L. Gardossi, Nature inspired solutions for polymers: will cutinase enzymes make polyesters and polyamides greener? Catalysts 6 (2016) 205, https://doi.org/10.3390/catal6120205.
[69] Q.Y. Huang, S. Kimura, T. Iwata, Thermal embedding of humicola insolens cutinase: a strategy for improving polyester biodegradation in seawater, Biomacromolecules 24 (2023) 5836–5846, https://doi.org/10.1021/acs.biomac.3c00835.